AGU PUBLICATIONS

JGR

Journal of Geophysical Research: Biogeosciences

RESEARCH ARTICLE
10.1002/2015JG003147

Key Points:
- We evaluated low-temperature, anoxic decomposition of tundra soil organic matter
- Fermentation supplied substrates for concomitant Fe reduction and methanogenesis
- Identified pathways are important for predicting C emissions from Arctic soils

Supporting Information:
- Supporting Information S1

Correspondence to:
E. M. Herndon and B. Gu,
eherndo1@kent.edu;
gub1@ornl.gov

Citation:
Herndon, E. M., B. F. Mann, T. Roy Chowdhury, Z. Yang, S. D. Wullschleger, D. Graham, L. Liang, and B. Gu (2015), Pathways of anaerobic organic matter decomposition in tundra soils from Barrow, Alaska, *J. Geophys. Res. Biogeosci.*, *120*, 2345–2359, doi:10.1002/2015JG003147.

Received 10 JUL 2015
Accepted 25 OCT 2015
Accepted article online 28 OCT 2015
Published online 23 NOV 2015

Pathways of anaerobic organic matter decomposition in tundra soils from Barrow, Alaska

Elizabeth M. Herndon[1,2], Benjamin F. Mann[1], Taniya Roy Chowdhury[3], Ziming Yang[1], Stan D. Wullschleger[1], David Graham[3], Liyuan Liang[1], and Baohua Gu[1]

[1]Environmental Sciences Division, Oak Ridge National Laboratory, Oak Ridge, Tennessee, USA, [2]Now at Department of Geology, Kent State University, Kent, Ohio, USA, [3]Biosciences Division, Oak Ridge National Laboratory, Oak Ridge, Tennessee, USA

Abstract Arctic tundra soils store a large quantity of organic carbon that is susceptible to decomposition and release to the atmosphere as methane (CH_4) and carbon dioxide (CO_2) under a warming climate. Anaerobic processes that generate CH_4 and CO_2 remain unclear because previous studies have focused on aerobic decomposition pathways. To predict releases of CO_2 and CH_4 from tundra soils, it is necessary to identify pathways of soil organic matter decomposition under the anoxic conditions that are prevalent in Arctic ecosystems. Here molecular and spectroscopic techniques were used to monitor biological degradation of water-extractable organic carbon (WEOC) during anoxic incubation of tundra soils from a region of continuous permafrost in northern Alaska. Organic and mineral soils from the tundra active layer were incubated at −2, +4, or +8°C for up to 60 days to mimic the short-term thaw season. Results suggest that, under anoxic conditions, fermentation converted complex organic molecules into simple organic acids that were used in concomitant Fe-reduction and acetoclastic methanogenesis reactions. Nonaromatic compounds increased over time as WEOC increased. Organic acid metabolites initially accumulated in soils but were mostly depleted by day 60 because organic acids were consumed to produce Fe(II), CO_2, and CH_4. We conclude that fermentation of nonprotected organic matter facilitates methanogenesis and Fe reduction reactions, and that the proportion of organic acids consumed by methanogenesis increases relative to Fe reduction with increasing temperature. The decomposition pathways observed in this study are important to consider in numerical modeling of greenhouse gas production in the Arctic.

1. Introduction

Rapidly changing climate at high latitudes is driving pronounced and complex shifts in polar environments [*Hinzman et al.*, 2013]. Ongoing changes in land cover, soil temperature, thaw depth, and water saturation are expected to influence rates and pathways of organic matter decomposition, potentially increasing releases of greenhouse gases (GHG) such as carbon dioxide (CO_2) and methane (CH_4) into the atmosphere [*Hinzman et al.*, 2005; *Schuur et al.*, 2008; *Tarnocai et al.*, 2009; *Koven et al.*, 2011]. Extensive efforts are underway to model how carbon (C) budgets in the Arctic will respond to climate change [*McGuire et al.*, 2009]; however, biogeochemical processes in tundra soils represent a source of major uncertainty in predicting land-climate feedbacks [*Riley et al.*, 2011; *Graham et al.*, 2012]. To improve predictions of CO_2 and CH_4 fluxes, it is necessary to understand the unique processes that occur in Arctic soils, including anaerobic decomposition of organic matter [*Riley et al.*, 2011], microbial respiration at near-freezing temperatures [*Michaelson and Ping*, 2003], and nonlinear, threshold responses to thawing [*Mikan et al.*, 2002; *Schimel and Mikan*, 2005; *Roy Chowdhury et al.*, 2015].

Arctic tundra soils are organic rich due to accumulation of slowly decomposing plant material over thousands of years. Rising temperatures are expected to accelerate decomposition by increasing rates of microbial metabolism and thawing previously frozen soil organic carbon (SOC) at depth. Radiocarbon dating has shown the signature of old soil C stocks in CO_2 released from the Arctic tundra [*Schuur et al.*, 2009], suggesting that warming-induced processes (e.g., permafrost subsidence and increased thaw depth) increase the availability of older, previously frozen organic matter for microbial degradation. The magnitude and relative proportion of CO_2 and CH_4 released from decomposition reactions are likely to vary across geomorphic features due to differences in water saturation and microbial community compositions [*Smith et al.*, 2005; *Schuur et al.*, 2008; *Mackelprang et al.*, 2011; *Sturtevant and Oechel*, 2013]. For example, thawing of permafrost can drain lakes and water-saturated soils to create oxic conditions in the active layer that facilitate rapid

decomposition and enhanced CO_2 release [*Huemmrich et al*., 2010; *Liljedahl et al*., 2012; *Elberling et al*., 2013]. Conversely, soil saturation may increase in areas of continuous permafrost, shifting active layers toward anaerobic respiration and methanogenesis pathways [*Turetsky et al*., 2008; *Zona et al*., 2009; *Lipson et al*., 2012; *Olefeldt et al*., 2013; *Intergovernmental Panel on Climate Change*, 2014]. Although SOC is largely stored under anoxic conditions in the Arctic, few studies examine anaerobic decomposition processes [e.g., *Roy Chowdhury et al*., 2015; *Treat et al*., 2015] while most focus on aerobic processes [e.g., *Weintraub and Schimel*, 2003; *Schädel et al*., 2014]. Thus, examining anaerobic decomposition pathways can improve our understanding of CO_2 and CH_4 production, particularly in persistently saturated soils that are prevalent in areas of continuous permafrost.

In this study, we monitored substrates and products of anaerobic decomposition reactions in laboratory incubations of tundra soils. We examined nonamended soil organic matter (SOM) decomposed under environmentally relevant temperatures (−2, +4, and +8°C) that span the range of soil temperatures measured during the thaw season in Barrow, AK. We hypothesized that chemical changes in water-extractable organic carbon (WEOC), which consists primarily of readily soluble organic acids, carbohydrates, and microbial metabolites [e.g., *Boyer and Groffman*, 1996; *Jandl and Sollins*, 1997; *Shaver et al*., 2006], would indicate decomposition pathways underlying the production of CO_2 and CH_4 reported for these incubations [*Roy Chowdhury et al*., 2015]. We expected that the rate of decomposition, measured as declines in WEOC and organic acid concentration over time, would increase with increasing temperature. Spectroscopic techniques were used to probe changes in the bulk chemical properties of WEOC during SOM decomposition. Changes in individual intermediate compounds that are precursors for GHG production (e.g., acetate) were analyzed to further evaluate mechanisms and pathways of CO_2 and CH_4 production.

2. Materials and Methods

2.1. Site Description

The Barrow Environmental Observatory (BEO) is located in the Arctic coastal plain of northern Alaska in the United States. The coastal plain has minimal topographic relief and is dominated by lakes and polygonal ground features that develop as ice wedges form [*Brown et al*., 1980; *Hinkel et al*., 2005]. Although mean annual precipitation is low (12 cm yr^{-1} rainfall + 75 cm yr^{-1} snowfall) [*Western Regional Climate Center*, 2015], the landscape is largely water saturated with poor drainage due to underlying permafrost [*Bockheim et al*., 1999]. Shallow ground (<1.2 m depth) temperatures in the region range from approximately −22°C in the winter to 4°C in the summer, and temperature fluctuations are more pronounced near the soil surface than at depth [*Shiklomanov et al*., 2010]. Maximum thaw depth in the tundra active layer ranges from ~21 to 58 cm (average 36 cm) across the landscape [*Hubbard et al*., 2013].

This study focuses on a low-centered polygon in an interstitial area examined as part of the Next Generation Ecosystem Experiment (NGEE) Arctic project [*Wullschleger et al*., 2011; *Hubbard et al*., 2013]. Soils in low-centered polygons are typically organic rich, water saturated, and persistently anoxic at depth [*Bockheim et al*., 1999; *Lipson et al*., 2010; *Zona et al*., 2011]. During the summer thaw season, the low-centered polygon investigated here (~40 m diameter) is characterized by narrow, saturated troughs that border the polygon, relatively high and dry topographic ridges, and a depressed and saturated polygon center (Figure 1). These microtopographic features generate vertical redox gradients over centimeter scales, as measured in a nearby drained thaw lake basin [*Zona et al*., 2011].

Frozen soil cores were obtained from center, ridge, and trough topographic positions of the low-centered polygon in April 2012. A Snow, Ice, and Permafrost Research Establishment coring auger (manufactured by Jon's Machine Shop in Fairbanks, AK) mounted on a sled was used to collect ~1 m length soil cores in clear PVC liners (3″ diameter times 36″ length) that were sterilized with ethanol prior to use. Soil cores were kept frozen during shipment to and storage at Oak Ridge National Laboratory.

2.2. Laboratory Incubation Experiment

Frozen soil cores were removed from their liners under N_2 atmosphere in a glove box to maintain anoxic conditions. All equipment was sterilized with ethanol during soil processing. Each soil core was sectioned into organic and mineral horizons that were subsequently thawed and homogenized in a plastic bucket using an oscillating power tool with sterilized cutting blades. Organic horizon thickness ranged from 8 to 22 cm while the mineral horizons extended to depths of 46 to 69 cm (Figure 1). Ground ice was present at the bottom of

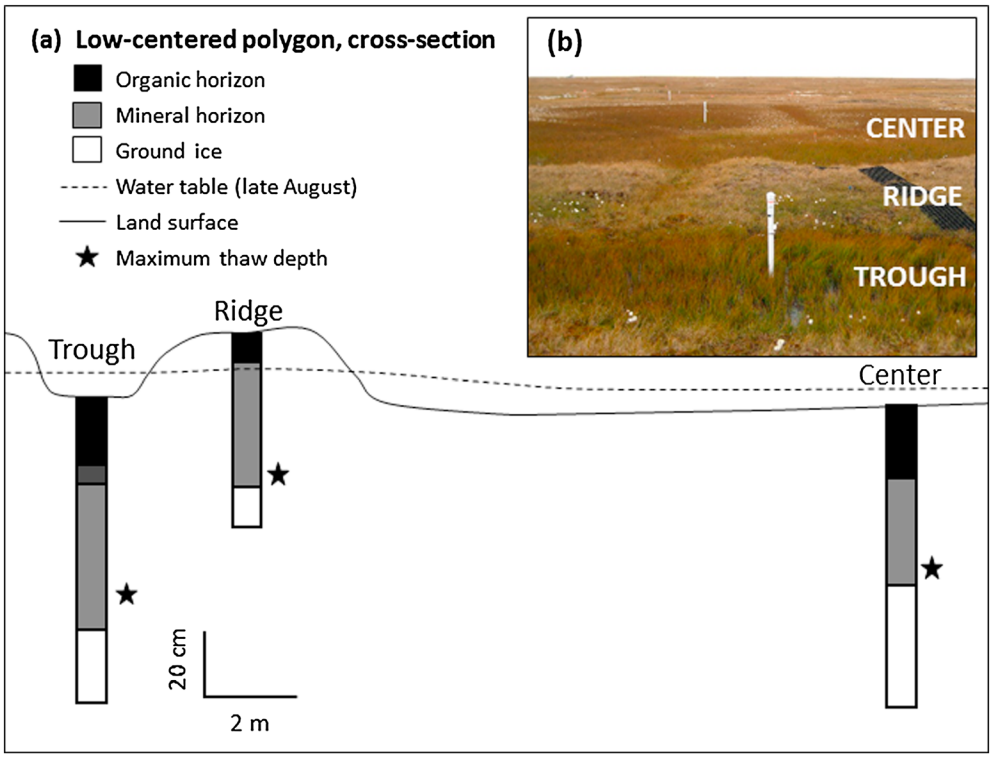

Figure 1. (a) A diagram of a low-centered polygon is shown in cross section from the land surface. Shaded vertical bars designate the relative landscape positions of the soil cores collected in April 2012 and used in this study as well as the depths of organic (black) and mineral (grey) horizons and ice layers (white) in each core. The center core was collected from the middle of the depressed center of the low-centered polygon. The properties of each horizon are given in Table 1. The dashed line indicates the approximate height of the water table measured in late August 2013. The scales of the vertical and horizontal dimensions of the low-centered polygon are indicated. (b) Topographic positions are indicated on a photograph of the low-centered polygon from late August 2013.

all cores at depths just below the maximum thaw depth measured in early September 2012 (Figure 1); thus, collected soils were almost entirely within the active layer of the tundra. Bottom layers containing predominantly ice were excluded from further processing.

A subset of microcosms was immediately refrozen at −20°C (incubation time = 0 days). The remaining microcosms were incubated at −2°C, 4°C, or 8°C for either 30 or 60 days prior to destructive sampling. The organic horizon of the ridge soil (RO) was only incubated for 30 days due to limited sample quantity. Incubation temperatures were selected to represent the range of soil temperatures measured during the thaw season at the BEO [*Hinkel et al*., 2001]. Thirty day time intervals were chosen to ensure observable changes in organic carbon chemistry. Aliquots (0.5 mL) of microcosm headspace were sampled every 2–5 days for 60 days and analyzed for CO_2 and CH_4 on a SRI 8610C gas chromatograph equipped with a Methanizer and Flame Ionization Detector, as reported by *Roy Chowdhury et al*. [2015]. To quantify exchangeable Fe(II), subsamples of soils (t = 0 or 30 days) were extracted with 2 M KCl (1:5 w/v) under anoxic conditions for 1 h, and then the extract was filtered (0.2 μm nylon filter) and immediately analyzed by measuring the 510 nm absorbance after reaction with a Hach FerroVer 1,10-phenanthroline chemical assay (method 8146) [*Roy Chowdhury et al*., 2015].

Following incubation, soils from the microcosms were transferred to 50 mL Falcon tubes under a N_2 atmosphere in the glove box, refrozen at −20°C, and then freeze-dried for 48 h. Soil water content was measured as mass loss from the frozen soil during freeze drying and was consistent with values obtained from replicate samples that were oven dried overnight at 105°C. To obtain water-extractable organic carbon (WEOC), ~1 g of ground, freeze-dried soil was mixed with 20 mL of a dilute electrolyte solution prepared in 18 MΩ water (0.01 M KCl, measured pH = 4.5) in a 50 mL Falcon tube at room temperature for ~20 h (modified from *Boyer and Groffman* [1996], *Jandl and Sollins* [1997], and *Hishi et al*, [2004]). Differences in the amount of organic C extracted by this dilute electrolyte solution are expected to be negligible relative to ultrapure water

extractions based on similar extractions of arctic tundra soils reported by *Hobara et al.* [2013]. As determined in a control experiment, concentrations of organic acid metabolites showed minor increases (<10%) from 1 to 20 h of extraction time (Figure S1 in the supporting information). These results confirm that decomposition of WEOC by contaminant microorganisms did not occur during the extraction. Supernatant was collected following centrifugation for 30 min at 7000 × *g*. Soils were rinsed twice by vortexing the pellet with ~10 mL 0.01 M KCl solution, centrifuging for 20 min at 7000 × *g*, and combining the rinse with the extract. All extracts were stored at 4°C until analysis. The extraction procedure yielded < 3% variance in the concentration of WEOC, as determined by conducting duplicate extractions of four different soil samples (Table S1).

2.3. Chemical Characterization of Water-Extractable Organic Carbon

Concentrations of total dissolved organic carbon (DOC) were determined for WEOC solutions, method blanks, and analytical blanks acidified with 0.5% ultrapure hydrochloric acid and analyzed on a Shimazdu TOC-L (Shimazdu Corp., Japan). The total organic carbon content of bulk soil was measured by combustion on a LECO TruSpec CN Determinator (LECO Corp., Michigan). Carbon concentrations in extract solutions were normalized to the mass of freeze-dried soil (μmol C g soil^{-1}). For comparison across soils, WEOC is also presented normalized to the mass of soil organic C (μmol C g SOC^{-1}).

Chemical properties of the WEOC were evaluated using ultraviolet-visible and Fourier transform infrared spectroscopies. For ultraviolet-visible spectrophotometry (UV-vis), soil extracts were diluted, as appropriate, in dilute sodium bicarbonate solution and transferred to a quartz cuvette before analysis. Absorbance was recorded in the range 200 to 800 nm on a Hewlett-Packard 8453 spectrophotometer using ultrapure water as an instrument blank. A method blank (0.01 M KCl solution) was measured to have negligible absorbance in this range.

Fourier transform infrared (FTIR) spectra were obtained from 4000 to 800 cm^{-1} at 2 cm^{-1} steps on a Nicolet Magna 760 spectrophotometer equipped with a liquid nitrogen cooled MCT (Mercury-Cadmium-Tellurium) detector [*Chen et al.*, 2002]. Extract solutions were deposited on ZnSe windows and dried in an oven at 60°C prior to analysis. For extracts with low DOC concentrations, samples were concentrated by depositing multiple layers on the window. All spectra were background corrected against a clean ZnSe window. Relative intensities of absorbance peaks at specific wavenumbers were determined following baseline subtraction using Thermo Nicolet OMNIC v7.3 software.

Previously established indices from multiple spectroscopic techniques were used to examine initial and changing chemical characteristics of WEOC during incubations. Specifically, indices included are as follows:

1. UV-vis: $SUVA_{254}$ (L mg C^{-1} m^{-1}), the absorptivity at 254 nm, for which higher values indicate a higher percent aromaticity in the dissolved C [*Chen et al.*, 2002; *Weishaar et al.*, 2003; *Stolpe et al.*, 2013]. Absorption in the UV range is attributed to the presence of delocalized pi-bonded (aromatic) and nonbonded electrons (e.g., O, N, and S containing moieties), while highly conjugated chromophoric molecules absorb in the visible range [*Swift*, 1996]. $SUVA_{254}$ is provided in mass units as reported in the literature [*Weishaar et al.*, 2003; *Stolpe et al.*, 2013].
2. UV-vis: $A_{265/465}$, the ratio of absorptivity at 265 to 465 nm, for which lower values indicate a higher degree of humification and functional groups that absorb more strongly in the visible region (e.g., highly conjugated polyaromatic molecules) relative to the ultraviolet region [*Swift*, 1996; *Chen et al.*, 2002].
3. FTIR: Ratios of IR peak intensity at ~1040 cm^{-1} and ~1400 cm^{-1} relative to ~1640 cm^{-1} as indicators of the proportion of C–O functional groups contained in carbohydrates or polysaccharides and carboxylic acids, respectively, relative to aromatic C = C and C = O functional groups [e.g., *Solomon et al.*, 2005].

Low-molecular weight organic acids were analyzed with ion chromatography. For each extract solution, a 10 μL aliquot was loaded onto a Dionex AS15 analytical column functionalized with a quaternary ammonium stationary phase. A multistep gradient of increasing sodium hydroxide from 10 mM up to 80 mM was applied to the column with a Dionex EG40 eluent generator to elute organic acids. Calibration curves for the measured organic acid anions were generated with standard compounds, including acetate, formate, propionate, butyrate, succinate, tartrate, oxalate, fumarate, oxoglutarate, and citrate. Lactate, another product of fermentation, was observed in some of the samples, though it could not be quantified due to overlap with the much larger acetate peak.

Table 1. Properties of the Organic and Mineral Horizons of Three Representative Soil Cores From Trough, Ridge, and Center Microtopographic Features of a Low-Center Polygon

NGEE ID	Position	Horizon	Layer Depth (cm)	Water Content ($g\ H_2O\ g^{-1}$ soil)	SOC (C wt %)
NGADG0009-1	Trough	Organic	0–19	2.48	20.5
NGADG0005-1	Ridge	Organic	0–8	3.67	38.9
NGADG0017-1	Center	Organic	0–21.5	9.62	38.3
NGADG0009-2	Trough	Mineral	25–69	0.79	8.0
NGADG0005-2	Ridge	Mineral	8–46	0.74	14.6
NGADG0017-2	Center	Mineral	21.5–53.5	0.64	13.8

Dissolved organic compounds in WEOC from two soils (ridge organic and center mineral soils) were resolved using high performance liquid chromatography (HPLC) coupled to ultraviolet detection at 260 nm (A_{260}; mAU). This method was used to semiquantitatively evaluate changes in organic compounds over the time course of the incubation experiments. Peaks in the chromatogram are proportional to concentrations of individual compounds. Compounds that could not be eluted with 95% acetonitrile were not detected, as they irreversibly bound to the guard column at the beginning of each analysis. All chromatograms were baseline subtracted and normalized to initial soil mass to yield an absorption unit (AU g $soil^{-1}$). Although individual compounds were not identified, the organic molecules were classified based on their polarity due to their retention on the C18 column, with longer retention times corresponding to decreased compound polarity.

2.4. Statistical Analysis

Statistical tests were performed in OriginPro software (OriginLab®). One-way repeated measures analysis of variance (ANOVA) was used to test the effect of incubation time on concentrations of water-extractable organic carbon and organic acids. The ridge organic soil was not included because no data were available for $t = 60$ days. The effects of incubation temperature (−2°C, 4°C, or 8°C) and soil horizon (organic or mineral)

Table 2. Concentrations of WEOC Normalized to Either the Mass of Soil (μmol g $soil^{-1}$) or Soil Organic Carbon (μmol g SOC^{-1})

		WEOC					
		μmol g $soil^{-1}$			μmol g SOC^{-1}		
Soil Feature/Horizon	Temperature (°C)	0 days	30 days	60 days	0 days	30 days	60 days
Trough, Organic	−2	64.2	86.7	108	313	423	527
Trough, Organic	4		103	141		502	688
Trough, Organic	8		122	96.7		595	472
Trough, Mineral	−2	20	40	37.5	250	501	469
Trough, Mineral	4		30.8	18.3		385	229
Trough, Mineral	8		28.3	27.5		354	344
Ridge, Organic	−2	176	206	n.a.	452	529	n.a.
Ridge, Organic	4		251	n.a.		645	n.a.
Ridge, Organic	8		242	n.a.		622	n.a.
Ridge, Mineral	−2	31.7	38.3	22.5	217	262	154
Ridge, Mineral	4		35	33.3		239	228
Ridge, Mineral	8		31.7	34.2		217	234
Center, Organic	−2	565[a]	724	579	1480[a]	1,890	1,510
Center, Organic	4		629	613		1640	1,600
Center, Organic	8		670	598		1750	1,560
Center, Mineral	−2	35	35.8	30.8	254	259	223
Center, Mineral	4		36.7	40		266	289
Center, Mineral	8		33.3	25.8		241	187

[a]For the center organic horizon, the concentration of WEOC was not available for $t = 0$ days; therefore, WEOC at $t = 0$ days was estimated as the average concentration of nonorganic acid C ($C_{WEOC} - C_{OA}$) for 30 and 60 days (1290 ± 149 μmol C g^{-1} SOC) plus the concentration of C contained in organic acids at $t = 0$ days (183 μmol C g^{-1} SOC). WEOC, Water-Extractable Organic Carbon; n.a., not available.

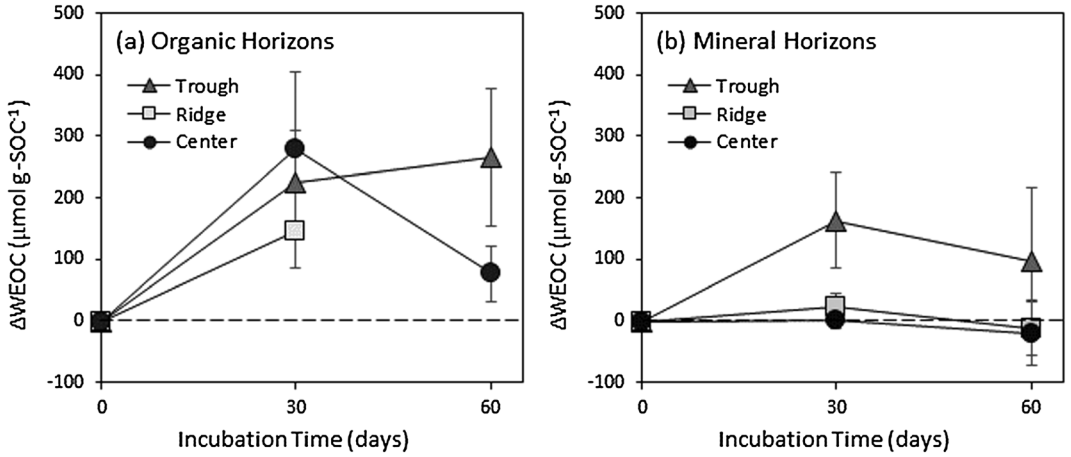

Figure 2. Changes in water-extractable organic carbon (WEOC) in (a) organic horizon and (b) mineral horizon soils incubated for 30 and 60 days are shown relative to concentrations in the nonincubated soils (ΔWEOC, μmol C g SOC^{-1}). Symbols and error bars represent the averages and standard deviations of three microcosms for each soil at each time point.

on changes in WEOC and organic acid concentrations from 0 to 30 days were tested with Kruskal-Wallis ANOVA. Mean comparisons were evaluated using Tukey's honest significant difference post hoc test. Effects were determined to be statistically significant to a level $\alpha = 0.05$. The effect of topographic feature could not be determined due to lack of site replication.

3. Results

3.1. Water-Extractable Organic Carbon

Mineral horizon soils were organic rich (8–15 wt % C) but lower in C content than organic horizon soils, which were composed almost entirely of organic matter (21–38 wt % C) (Table 1). The gravimetric water content of the organic horizons soils (2.5–9.6 g H_2O g^{-1} soil) exceeded the mineral soils (0.6–0.8 g H_2O g^{-1} soil) due to a high concentration of low-density organic matter that yielded greater porosity and higher ratios of water to dry soil mass. Although the organic horizons of the center and ridge soils had similar weight percent C, the ridge exhibited substantially lower water content, indicating that the ridge soil was less saturated. This result was in agreement with observations made during the summer thaw season, when the water table is above the land surface in trough and center locations but below the organic horizon at the ridge (Figure 1).

Prior to incubation (i.e., time = 0 days), WEOC comprised $< 2\%$ of the total SOC and was higher in organic (313–1480 μmol g SOC^{-1}) than mineral horizons (217–254 μmol g SOC^{-1}) (Table 2). Changes in WEOC (ΔWEOC, μmol C g SOC^{-1}) were evaluated after 30 and 60 days of incubation relative to nonincubated soils. WEOC varied as a function of time across all soils ($p = 0.002$) and generally increased from 0 to 30 days. Soil horizon ($p = 0.01$), but not incubation temperature ($p > 0.05$), impacted ΔWEOC. Given that temperature was not a significant factor influencing changes in WEOC, data collected at all three temperatures were averaged for each soil at each time point in Figure 2. WEOC increased in organic soils of the ridge (ΔWEOC = 147 ± 61 μmol C g SOC^{-1}), trough (ΔWEOC = 194 ± 86), and center (ΔWEOC = 285 ± 124) features from 0 to 30 days before decreasing (Figure 2a). WEOC also increased in the trough mineral soil (ΔWEOC = 163 ± 77 μmol C g SOC^{-1}) but did not change in the ridge or center mineral soils (Figure 2b).

3.2. Spectroscopic Characterization of WEOC

$SUVA_{254}$ values for WEOC ranged from 1.0 to 6.0 L mg C^{-1} m^{-1} and were consistent with values previously reported for WEOC from tundra soil [*Dou et al.*, 2008], and for DOC in Alaskan rivers (2.3–4.3 L mg C^{-1} m^{-1}) [*Stolpe et al.*, 2013] and in rivers draining large watersheds (>1000 km^2) throughout the conterminous United States (1.3–4.7 L mg C^{-1} m^{-1}) [*Hanley et al.*, 2013]. WEOC from the mineral horizons contained more aromatic and conjugated molecules per unit mass C than WEOC from the organic horizons, as indicated by higher $SUVA_{254}$ and lower $A_{265/465}$ values (Figures 3a and 3c). Thus, WEOC from mineral soil was more similar

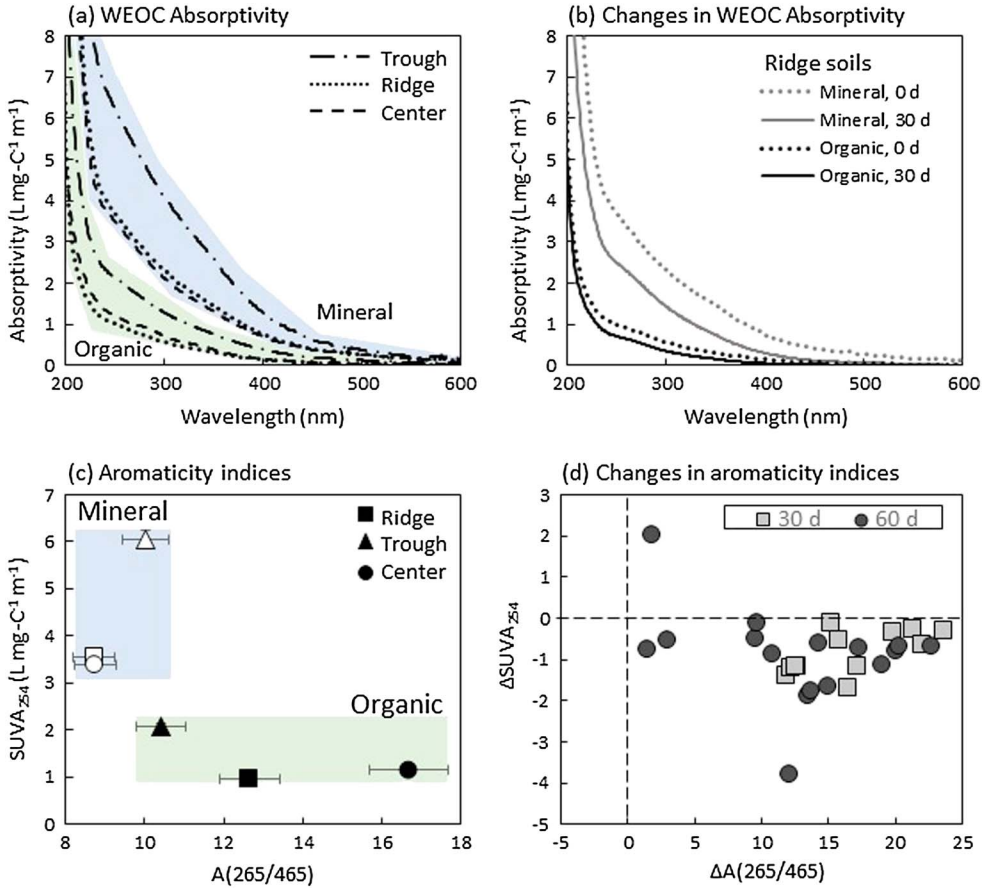

Figure 3. Ultraviolet-visible spectral properties of water-extractable organic C (WEOC) indicated a decrease in aromatic character during laboratory incubation of soils collected from trough, ridge, and center topographic features in a low-centered polygon. (a) Prior to incubation, absorptivity (L mg C^{-1} m^{-1}) of WEOC was higher in the mineral horizons (blue area) than the organic horizons (green area). (b) The absorptivity of WEOC decreased during incubation, as shown here for the organic (black lines) and mineral horizon (grey lines) of the ridge soil incubated for $t = 0$ (dashed lines) and $t = 30$ d at 8°C (solid lines). (c) Aromaticity indices, $SUVA_{254}$ and A(265/465), indicated that WEOC from mineral horizons (open symbols) was more aromatic than WEOC from organic horizons (filled symbols). (d) Changes (Δ) in WEOC aromaticity indices following incubation were determined relative to nonincubated soils. Values in the lower right quadrant indicated a decrease in the aromatic properties of WEOC. Shaded regions in Figures 3a and 3c delineate the boundaries of measured values.

to humic acid fractions ($SUVA_{254} > 5$ L mg C^{-1} m^{-1}) [*Weishaar et al.*, 2003] than WEOC from organic soils which was more similar to fulvic acid and carbohydrate-rich organic fractions ($SUVA_{254} < 4$ L mg C^{-1} m^{-1}) [*Weishaar et al.*, 2003; *Chen et al.*, 2002].

Following incubation, $SUVA_{254}$ of WEOC decreased ($\Delta SUVA_{254} = -0.1$ to -3.8 L mg C^{-1} m^{-1}) and A_{265}/A_{465} increased ($\Delta A_{265}/A_{465} = 1.5$ to 23.6) for nearly all samples (Figures 3b and 3d). Using $SUVA_{254}$ as a proxy for aromaticity [e.g., *Weishaar et al.*, 2003], the changes in $SUVA_{254}$ corresponded to a decrease of roughly 4–28% aromatic C in the WEOC pool. These trends are consistent with an increase in the proportion of carbohydrate-rich C and a decrease in the proportion of soil humic acids and polyphenolic-rich C contained in WEOC over time [*Chen et al.*, 2002].

For all nonincubated soils, FTIR spectra for WEOC were dominated by absorbance peaks representing hydroxyl (~3400 cm^{-1}) and aromatic C = C and carbonyl C = O (~1640 cm^{-1}) functional groups (Figure 4a). Following incubation, absorbance peaks consistent with C–O functional groups and indicative of carboxylic acids + phenols (~1400 cm^{-1}) and polysaccharides (~1040 cm^{-1}) increased relative to the 1640 cm^{-1} peak, while hydroxyl peak decreased in intensity and broadened (Figures 4b and 4c). Aliphatic $CH_2 + CH_3$ peaks (2850 and 2920 cm^{-1}) increased in some samples, but the changes were small and difficult to discern. Figure 4b illustrates a time series in IR spectra using WEOC from the trough mineral soil as an example, and similar

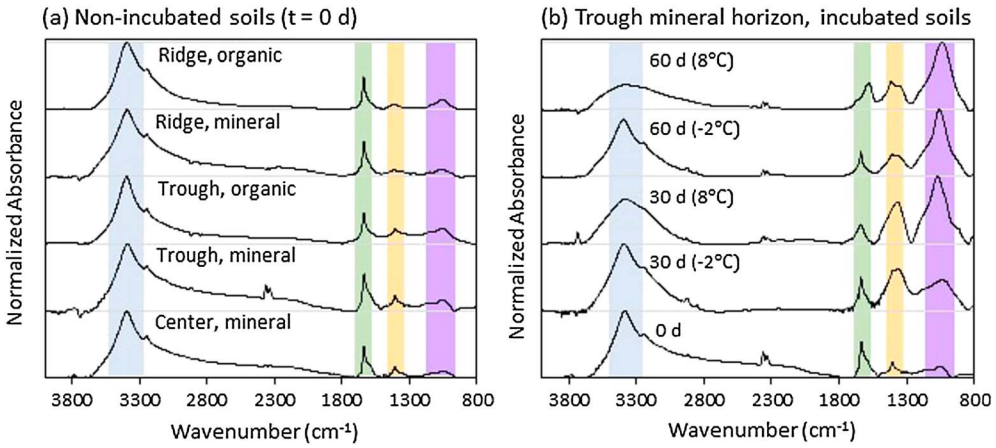

Figure 4. Absorption peaks in the Fourier transform infrared spectra of water-extractable organic carbon indicate the presence of functional groups including O–H (~3400 cm^{-1}), C=C + C=O (~1640 cm^{-1}), C–O in carboxylic acids and phenolics (~1400 cm^{-1}), and C–O in polysaccharides and carbohydrates (~1040 cm^{-1}) [*Solomon et al.*, 2005]. These absorption peaks are highlighted for emphasis in Figures 4a and 4b. (a) IR spectra were similar for all nonincubated soils and dominated by O–H and C=C + C=O absorption peaks. (b) Peaks associated with C–O groups (orange and purple bars) increased during incubations, as shown here in the time series of spectra from the trough mineral horizon incubation and in the supporting information (Figure S2) for all other samples.

increases in 1400/1640 and 1040/1640 peak ratios were observed in WEOC extracted from all organic and mineral soil microcosms (Figure S2).

The suite of organic compounds detected using HPLC differed for two soil extracts (WEOC from the ridge organic and center mineral soils) with minor changes during incubations (Figure S3). These compounds were considered more nonpolar than the organic acids in these samples (described below) and represented a potential source of precursors for metabolite production. In each sample, a large peak was observed shortly after injection, indicating the presence of polar compounds that were not retained on the column. Compounds detected by HPLC-UV exhibited fewer changes in mineral horizon extracts than in organic horizon extracts during incubations. Furthermore, the organic soil exhibited mostly increases in individual

Table 3. Concentrations of Individual Organic Acids in Water-Extractable Organic Carbon Normalized to Soil Organic Carbon (μmol g SOC^{-1}) for Soils Incubated for 0, 30, or 60 days[a]

		Formate			Acetate			Propionate			Butyrate		
Soil Horizon	Temperature (°C)	0 days	30 days	60 days	0 days	30 days	60 days	0 days	30 days	60 days	0 days	30 days	60 days
Ridge organic	−2	0.08	0.11		0.08	0.94		0.08	0.08		< DL	< DL	
	4		0.08			0.04			0.08			< DL	
	8		0.55			6.11			1.93			< DL	
Trough organic	−2	0.15	0.08	0.29	0.15	0.99	0.99	0.15	0.40	0.15	< DL	< DL	< DL
	4		3.55	0.09		29.2	0.45		7.43	0.15		< DL	< DL
	8		3.00	0.11		29.2	0.80		13.53	0.15		< DL	< DL
Center organic	−2	48.6	5.51	5.72	66	114	99.2	0.76	11.2	11.7	< DL	43.6	37.1
	4		7.10	0.08		154	22.1		17.0	19.0		31.2	18.9
	8		8.93	0.71		181	6.10		24.1	18.1		28.4	20.1
Ridge mineral	−2	1.78	1.83	0.21	5.6	5.55	0.21	0.29	2.60	0.21	< DL	< DL	< DL
	4		0.21	0.21		2.72	0.21		1.09	0.21		< DL	< DL
	8		0.21	0.21		1.40	0.21		2.10	0.21		< DL	< DL
Trough mineral	−2	2.54	1.85	0.38	8.1	8.12	0.38	0.14	2.95	0.38	< DL	< DL	< DL
	4		6.96	0.38		7.71	0.14		0.86	0.38		< DL	< DL
	8		1.36	0.38		9.02	0.38		4.22	0.38		< DL	< DL
Center mineral	−2	1.31	1.34	0.22	5.8	14.5	0.09	0.16	2.17	0.22	< DL	< DL	< DL
	4		1.36	0.22		12.1	0.19		2.39	0.22		< DL	< DL
	8		1.30	0.22		11.4	0.22		1.43	0.22		< DL	< DL

[a]For organic acids < LOQ in the extract solution, concentrations were calculated using LOQ = 0.06 μmol g^{-1} soil.

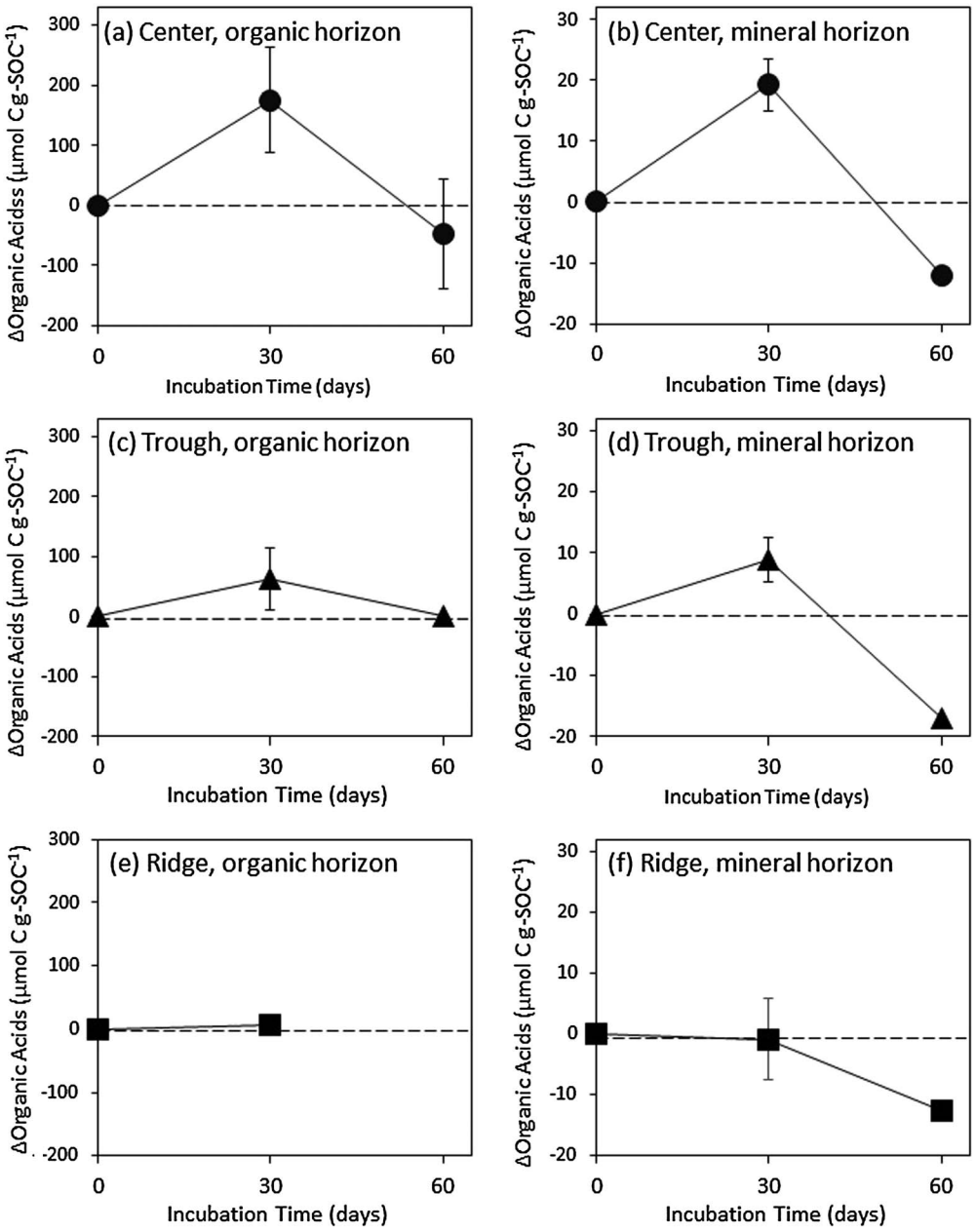

Figure 5. Changes in organic acid carbon concentrations (ΔOA, μmol C g SOC^{-1}) relative to concentrations in the non-incubated soils ($t = 0$ days) for (a, c, and e) organic horizon and (b, d, and f) mineral horizon soils incubated for 30 and 60 days. Symbols and error bars represent the averages and standard deviations for each soil across all three incubation temperatures (−2, +4, and +8°C). Note that the *y* axis range for Figures 5a, 5c, and 5e is an order of magnitude higher than for Figures 5b, 5d, and 5f.

compounds over time while the mineral soil exhibited mostly decreases. These results indicate that changes occurred in the nonpolar organic fraction during incubations, likely due to the breakdown of water-insoluble compounds and the subsequent degradation into smaller metabolites.

3.3. Organic Acids

While spectroscopic techniques provided a general assessment of WEOC chemistry, analyses of organic acids provided quantitative, compound-specific information on intermediate metabolites produced during microbial degradation of organic compounds to CO_2 and CH_4. Of all the organic acids analyzed, only the monocarboxylic acids formate, acetate, propionate, and butyrate were present in measureable quantities (>1 μM) in

Table 4. Changes in Concentrations of Acetate, Dissolved Ferrous Iron [Fe(II)], and Methane [CH_4] During the First 30 days of Incubation

Feature	Horizon	Temperature (°C)	ΔAcetate (μmol g SOC^{-1})	ΔFe(II)[a] (μmol g SOC^{-1})	ΔCH_4[b] (μmol g SOC^{-1})	Acetate Production[c] (μmol g SOC^{-1})	Acetate Consumed in Methanogenesis[c] (%)
Ridge	Organic	−2	0.86	154 ± 12	0.5 ± 0.1	21 ± 3	2.4 ± 0.6
		4	−0.03	169 ± 30	1.9 ± 0.9	23 ± 6	8.3 ± 4.5
		8	6.03	181 ± 18	7.3 ± 1.1	36 ± 6	20 ± 4
Trough	Organic	−2	0.84	150 ± 77	0.4 ± 0.1	20 ± 11	2.0 ± 1.3
		4	29.1	222 ± 53	7.5 ± 0.9	64 ± 11	12 ± 3
		8	29.1	201 ± 107	12 ± 3	66 ± 20	18 ± 7
Center	Organic	−2	48.4	384 ± 8	4.3 ± 0.3	101 ± 7	2.6 ± 0.3
		4	87.7	296 ± 3	119 ± 11	244 ± 26	38 ± 5
		8	115	236 ± 184	166 ± 7	310 ± 49	44 ± 7
Ridge	Mineral	−2	−0.1	105 ± 28	0.7 ± 0.2	14 ± 5	3.6 ± 1.4
		4	−2.9	107 ± 14	10.3 ± 0.7	21 ± 4	39 ± 7
		8	−4.2	108 ± 33	22 ± 2	31 ± 8	59 ± 17
Trough	Mineral	−2	−0.2	432 ± 82	1.0 ± 0.2	55 ± 14	1.6 ± 0.5
		4	−0.4	515 ± 72	4.6 ± 0.5	69 ± 14	6.0 ± 1.3
		8	0.9	234 ± 115	9.7 ± 1.1	40 ± 18	20 ± 9
Center	Mineral	−2	8.7	163 ± 47	2.3 ± 0.2	31 ± 8	6.2 ± 1.7
		4	6.3	248 ± 34	2.8 ± 1.2	40 ± 8	6.1 ± 3.0
		8	5.5	403 ± 64	4.3 ± 0.7	60 ± 12	6.5 ± 1.7

[a]The 2 M KCl extractable Fe(II); standard deviations in Fe(II) concentrations reported by *Roy Chowdhury et al.* [2015].
[b]Changes and standard error in CH_4 calculated from CH_4 production functions reported by *Roy Chowdhury et al.* [2015].
[c]Calculated as % of available acetate from $t = 0$ to $t = 30$ days; uncertainty derived from propagated error for Fe(II), CH_4, and acetate (±6%) concentrations.

WEOC (Tables 2 and S2). Concentrations of dicarboxylates and tricarboxylates (tartrate, oxalate, fumarate, oxoglutyrate, and citrate) were negligible.

Prior to incubation, concentrations of formate (1.9 ± 0.5 μmol g SOC^{-1}), acetate (6.5 ± 1.2 μmol g SOC^{-1}), and propionate (0.20 ± 0.07 μmol g SOC^{-1}) varied by less than a factor of 2 across all mineral soils and comprised 6.5 ± 1% of the WEOC. In contrast, organic acid concentrations in the organic horizons were more variable: in the center soil, formate (48.6 ± 1.9 μmol g SOC^{-1}), acetate (66 ± 11 μmol g SOC^{-1}), and propionate (0.76 ± 0.37 μmol g SOC^{-1}) comprised ~12% of WEOC, whereas in the ridge and trough soils, all organic acids were below detection (<0.2 μmol g SOC^{-1}) at day 0 and were estimated to represent <0.5% of the WEOC (Table 3).

To facilitate comparison of changes in organic acids over time across all soils, the concentration of C contained in organic acids (C_{OA}, μmol C g SOC^{-1}) was calculated as the sum of C contained in formate, acetate, and propionate. Butyrate was not included because it was only detected in the center organic soils at 30 and 60 d (Table S2b). C_{OA} changed as a function of incubation time ($p = 0.02$) but not temperature ($p > 0.05$). Given that temperature effects were negligible, data collected at all three temperatures were averaged for each soil at each time point (Figure 5). C_{OA} generally increased from day 0 to 30 and decreased from day 30 to 60, although the magnitude of change in C_{OA} was more pronounced in the organic horizon than the mineral horizon and decreased from the center to the trough to the ridge soils (Figure 5). Given that these changes are normalized to the mass of soil organic C, we infer that environmental and biological factors rather than bulk C abundance impacted trends of organic acid production and consumption.

We further investigated decomposition pathways by evaluating changes in acetate, Fe(II), and CH_4 concentrations from day 0 to 30 (Table 4) [*Roy Chowdhury et al.*, 2015]. Acetate, which exhibited the most dynamic concentration changes of the measured organic acids (Table 3), is a product of fermentation and a primary substrate for Fe reduction and methanogenesis [*Lovley and Phillips*, 1988; *Metje and Frenzel*, 2007; *Bethke et al.*, 2011]. If we assume that acetate is the dominant substrate for these processes, then the amount of acetate produced by fermentation prior to 30 days can be approximated as the sum of accumulated acetate (i.e., the change in acetate concentration from $t = 0$ to $t = 30$ d) and the amount of acetate consumed in Fe-reduction and methanogenesis reactions. The latter is determined using reaction stoichiometry and production of Fe(II) and CH_4 reported by *Roy Chowdhury et al.* [2015] and summarized in Table 4. Specifically, each mole of acetate consumed produced either 1 mol of CH_4 or 8 mol of Fe(II) [e.g., *Bethke et al.*, 2011]. The total concentration of acetate available for consumption was calculated as the sum of acetate present at $t = 0$ days and acetate production from $t = 0$ to $t = 30$ days.

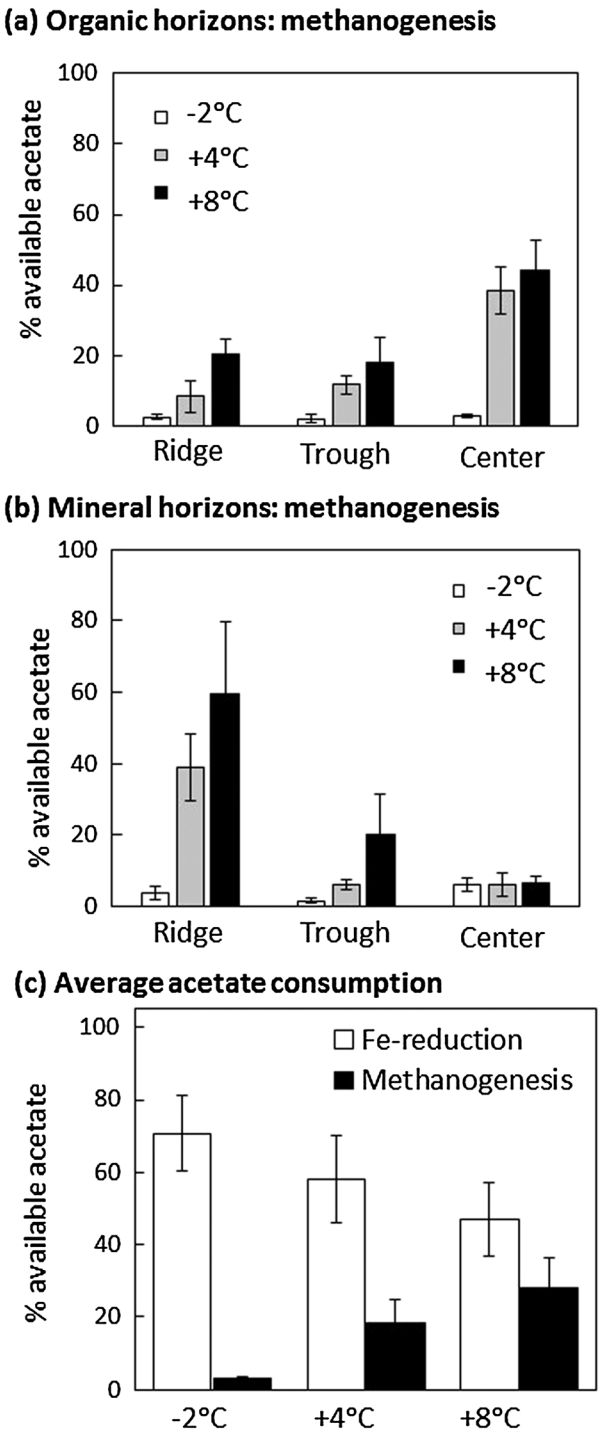

Figure 6. Acetate consumption in methanogenic pathways, defined as the percent of available acetate converted to methane from 0 to 30 days, increased with increasing temperature ($p = 0.005$) in the (a) organic and (b) mineral horizon soils. Available acetate was calculated as the sum of acetate present at $t = 0$ and the quantity of acetate produced from $t = 0$ to $t = 30$ days. Error bars indicate the propagated uncertainty in values used to calculate acetate production. (c) Percent of available acetate consumed in Fe-reduction (white bars) or methanogenesis (black bars) reactions from 0 to 30 days. Columns indicate the average ± standard error over all incubated soils at each temperature.

Temperature did not significantly influence acetate production during the first 30 days of incubation ($p > 0.05$); however, the percent of acetate consumed in methanogenesis reactions increased with increasing temperature ($p = 0.003$), using up to 60% of available acetate at 8°C but <7% at −2°C (Figures 6 and S4). The proportion of acetate consumed in Fe-reduction reactions ranged from 8 to 93% across all samples and showed no effect of temperature. In the organic horizon of the polygon center, which produced the most CO_2 and CH_4 [*Roy Chowdhury et al.*, 2015], methanogenesis consumed ~6 times more acetate (44%) than Fe reduction (8%) at 8°C but ~11 times less acetate (2.5%) than Fe reduction (29%) at −2°C. This pattern was observed in all soils except the mineral horizon of the polygon center, where Fe reduction consumed >54% and methanogenesis consumed 6 ± 2% of available acetate at all temperatures (Figure S4). These results suggest that methanogenesis used increasing amounts of acetate relative to Fe reduction with increasing temperatures over the first 30 days of incubation. After 30 days, organic acid concentrations decreased as available acetate was consumed (Figure 5 and Table 3).

4. Discussion

Anaerobic degradation of organic matter releases CO_2 and CH_4 to the atmosphere across the cold, water-saturated landscape of Arctic tundra. Here we provide spectroscopic and molecular evidence for microbial decomposition pathways that drive GHG releases. In our microcosm experiments, low-molecular weight organic acids initially accumulated in soils but were mostly depleted by day 60 of the incubations. A parallel study conducted on these microcosms reported decreasing CO_2:CH_4 ratios during this time due to declining rates of CO_2 production but steady to increasing rates of CH_4 production [*Roy Chowdhury et al.*, 2015]. We contend that observed trends are

explained by initially high rates of fermentation that produced organic acids and CO_2 from the breakdown of larger SOC molecules. Organic acids were subsequently consumed in concurrent methanogenesis and iron-reduction pathways, although the proportion of acetate consumed by each pathway varied as a function of temperature. Although all soils exhibited similar trends, rates of net organic acid production and consumption were more variable among organic horizon than mineral horizon soils.

4.1. Changes in Water-Extractable Organic Carbon During Incubations

Organic horizons had higher and more variable concentrations of WEOC than mineral horizons (Figure 2), and correspondingly higher rates of CO_2 and CH_4 production [*Roy Chowdhury et al*., 2015]. The center organic horizon, which released more GHG than any other soil [*Roy Chowdhury et al*., 2015], exhibited the highest and most dynamic concentrations of WEOC and organic acids (Figures 2 and 5). Similar to previous studies [*Michaelson and Ping*, 2003; *Treat et al*., 2015], this result indicates that the availability of easily degradable compounds present in WEOC may be one limiting factor in SOC degradation and GHG production. Conversely, only small to negligible changes in WEOC were observed in the mineral soil incubations. It is possible that the mineral soil horizons experienced a smaller degree of fermentation because advanced decomposition and mineral protection limited the availability of easily degraded substrates. This scarcity of excess fermentation products was apparent in the organic acid fraction, which either increased or decreased only slightly during the incubations (Figure 5).

Increases in WEOC were likely derived from partial decomposition of organic macromolecules. The degradation of more complex SOC molecules into water-soluble constituents explains CO_2 releases that were concurrent with small molecule production over the first 30 days of incubations. Precise determination of organic acid precursor molecules is challenging due to heterogeneous nature of SOC; however, HPLC-UV data provide initial evidence for production and degradation of nonpolar, metabolite precursor molecules in WEOC. Specifically, the ridge organic soil experienced mostly increases in water-extractable nonpolar compounds during incubation, whereas the center mineral soil experienced mostly decreases (Figure S2). These trends are consistent with the observation that WEOC increased in ridge organic soil but decreased in center mineral soil during this time (Figure 2).

Decreases in absorptivity ($SUVA_{254}$) and increases in A_{265}/A_{465} indicate that the proportion of aromatic and phenolic C decreased in the WEOC during incubations. While this decrease could indicate degradation of water-soluble aromatic compounds, concurrent increases in WEOC make these trends more consistent with an input of lower absorbing compounds, such as organic acids. Similar trends were observed in the IR data, where peaks associated with C–O functional groups increased over time but peaks associated with C=C and C=O functional groups did not change. Inputs of nonaromatic, C–O-rich compounds to the WEOC fraction likely represent the products of anaerobic oxidation fermentation of water-insoluble organic compounds. Our results are consistent with previous observations that an abundance of nonaromatic, low-molecular weight compounds generated during permafrost thaw and subsidence can increase CH_4 production potentials [*Hodgkins et al*., 2014].

4.2. Pathways of Anaerobic Decomposition

Previous studies conducted at the Barrow Environmental Observatory found that Fe(III) reduction was a dominate microbial metabolism in shallow, saturated tundra soils [*Lipson et al*., 2010; *Lipson et al*., 2013a; *Lipson et al*., 2013b]. *Roy Chowdhury et al*. [2015] observed that Fe(II) initially increased during laboratory incubations of the tundra soils examined in this study before reaching a plateau by day 30, consistent with initially high rates of microbial Fe(III) reduction that decreased over time. Our results indicated that methanogenesis and Fe reduction were concomitant prior to day 30; that is, acetate consumption by each process was approximately equal in soils incubated at 8°C (Figure 6). Methanogenesis was highly temperature dependent [*Roy Chowdhury et al*., 2015] and consumed an increasing proportion of available acetate with increasing temperature (Figure 6). In contrast, Fe reduction was variable and showed no effect of temperature. Although we cannot discount the possibility that organic compounds other than acetate were used to produce CH_4 and Fe(II), acetate is a major substrate in metabolic processes and was evaluated here to gauge the relative importance of these dominant metabolic pathways. We contend that methane was derived from acetate given that acetoclastic methanogenesis dominates methane production in BEO soils [*Throckmorton et al*., 2015] and other similar environments [e.g., *Metje and Frenzel*, 2007]; however, it is less certain if other compounds contributed to Fe(III) reduction in these incubations. If substrates other that acetate were used

to reduce Fe(III), as discussed below, then our calculations would overestimate acetate production and consequently underestimate acetate consumption in methanogenesis (as % of available acetate). Nitrate and sulfate concentrations were low in these soils [*Newman et al*., 2015; *Herndon et al*., 2015] and expected to have small to negligible impacts on microbial acetate consumption [*Lipson et al*., 2010].

Parallel Fe-reduction and methanogenesis processes have been previously demonstrated to occur in subarctic peat soils [*Metje and Frenzel*, 2007]. While Fe reduction may limit methane production in many environments [*Roden and Wetzel*, 1996; *Lipson et al*., 2012], the energetic yields of Fe reduction are strongly dependent on iron oxide mineralogy and pH, and rates of methanogenesis may exceed rates of Fe reduction in environments with low energetic yields [*Bethke et al*., 2011]. It is also possible that oxidation of complex molecules with Fe(III) may have facilitated methanogenesis by generating acetate and other organic acids. In highly decomposed systems, CH_4 production can be limited by substrate availability that depends on polysaccharide and lignin hydrolysis [*Shannon and White*, 1996; *Fey and Conrad*, 2003; *Weintraub and Schimel*, 2003], and Fe(III) reduction could facilitate initial oxidation of complex SOC [*Siegert et al*., 2011].

Coupled changes in acetate and methane concentrations indicate that methane was derived from acetate rather than CO_2 reduction. For example, soils that exhibited minimal changes in organic acid concentrations also exhibited minimal CH_4 production. If CO_2 were being reduced using H_2 generated during fermentation reactions, we would expect that organic acid fermentation products would accumulate rather than be depleted. Although previous studies report that the relative importance of methanogenic pathways can vary [*Kotsyurbenko et al*., 2004; *Metje and Frenzel*, 2007; *Hines et al*., 2008], acetoclastic methanogenesis has been exclusively demonstrated at 4°C [*Schulz and Conrad*, 1996] and may be the dominant pathway for methane production throughout the BEO [*Throckmorton et al*., 2015]. The coarse time points evaluated here could not be used to identify the timing of maximum accumulation or of net depletion of acetate; however, CO_2:CH_4 ratios stabilized at low values between 20 and 30 days for all samples, suggesting that the inflection point in acetate concentrations also occurred during this time. Future studies that examine changes in WEOC over shorter time intervals could provide valuable information on rates of substrate utilization for different decomposition pathways.

5. Conclusion

We provide evidence that warming-induced microbial degradation of SOC proceeds via fermentation pathways that facilitate methanogenesis and Fe reduction in anoxic Arctic tundra soils. These anaerobic processes were most pronounced in the saturated, organic horizon soils from the trough and center of the low-centered polygon. Decomposition reactions in the mineral horizon soils were relatively slow and similar across all topographic positions. Initial fermentation reactions produced water-soluble organic acids and carbohydrate-rich compounds, which were subsequently decomposed to carbon dioxide and methane gases. Although rates of fermentation did not appear to be temperature sensitive in this study, temperature did influence subsequent utilization of fermentation products. Specifically, methanogenesis consumed increasing amounts of acetate relative to Fe reduction with increasing temperatures. Our results indicate that warming of anoxic tundra soils could increase rates of SOC degradation, and particularly CH_4 and CO_2 production via acetoclastic methanogenesis, in organic horizons that contain abundant sources of nonprotected carbon. We suggest that this decomposition pathway be considered in numerical modeling of greenhouse gas production in the Arctic.

Acknowledgments
The authors would like to thank Kenneth Lowe for core sample collection, Xiangping Yin, Tonia Mehlhorn, and Deanne Brice for technical assistance and chemical analyses, and Lauren Kinsman-Costello and an anonymous reviewer for helpful discussion and comments. All data are available in the supporting information for this manuscript and in an online data repository (NGEE-Arctic Data Portal). The Next Generation Ecosystem Experiments (NGEE Arctic) project is supported by the U.S. Department of Energy (DOE) Office of Biological and Environmental Research. Oak Ridge National Laboratory is managed by UT-Battelle LLC for DOE under contract DE-AC05-00OR22725. Logistical support while working on the Barrow Environmental Observatory (BEO) was provided by Umiaq, LLC.

References

Bethke, C. M., R. A. Sanford, M. F. Kirk, Q. Jin, and T. M. Flynn (2011), The thermodynamic ladder in geomicrobiology, *Am. J. Sci.*, *311*, 183–210.
Bockheim, J. G., L. R. Everett, K. M. Hinkel, F. E. Nelson, and J. Brown (1999), Soil organic carbon storage and distribution in Arctic Tundra, Barrow, Alaska, *Soil Sci. Soc. Am. J.*, *63*, 934–940.
Boyer, J. N., and P. M. Groffman (1996), Bioavailability of water extractable organic carbon fractions in forest and agricultural soil profiles, *Soil Biol. Biochem.*, *28*(6), 783–790.
Brown, J., K. R. Everett, P. J. Webber, S. F. MacLean, and D. F. Murray (1980), The coastal tundra at Barrow, in *An Arctic Ecosystem: The Coastal Tundra at Barrow, Alaska*, edited by J. Brown et al., pp. 1–29, Dowden, Hutchinson and Ross, Stroudsburg, Pa.
Chen, J., B. Gu, E. J. Leboeuf, H. Pan, and S. Dai (2002), Spectroscopic characterization of the structural and functional properties of natural organic matter fractions, *Chemosphere*, *48*, 59–68.
Dou, F., C. L. Ping, L. Guo, and T. Jorgenson (2008), Estimating the impact of seawater on the production of soil water-extractable organic carbon during coastal erosion, *J. Environ. Qual.*, *37*(6), 2368–2374.
Elberling, B., A. Michelsen, C. Schädel, E. A. G. Schuur, H. H. Christiansen, L. Berg, M. P. Tamstorf, and C. Sigsgaard (2013), Long-term CO_2 production following permafrost thaw, *Nat. Clim. Change*, *3*, 890–894.

Fey, A., and R. Conrad (2003), Effect of temperature on the rate limiting step in the methanogenic degradation pathway in rice field soil, *Soil Biol. Biochem.*, *35*, 1–8.
Graham, D. E., et al. (2012), Microbes in thawing permafrost: the unknown variable in the climate change equation, *ISME J.*, *6*, 709–712.
Hanley, K. W., W. M. Wollheim, J. Salisbury, T. Huntington, and G. Aiken (2013), Controls on dissolved organic carbon quantity and chemical character in temperate rivers of North America, *Global Biogeochem. Cycles*, *27*, 492–504, doi:10.1002/gbc.20044.
Herndon, E. M., L. Jin, D. M. Andrews, D. M. Eissenstat, and S. L. Brantley (2015), Importance of vegetation for manganese cycling in temperate forested watersheds, *Global Biogeochem. Cycles*, *29*, 160–174, doi:10.1002/2014GB004858.
Hines, M. E., K. N. Duddleston, J. N. Rooney-Varga, D. Fields, and J. P. Chanton (2008), Uncoupling of acetate degradation from methane formation in Alaskan wetlands: Connections to vegetation distribution, *Global Biogeochem. Cycles*, *22*, GB2017, doi:10.1029/2006GB002903.
Hinkel, K. M., F. Paetzold, F. E. Nelson, and J. G. Bockheim (2001), Patterns of soil temperature and moisture in the active layer and upper permafrost at Barrow, Alaska: 1993–1999, *Global Planet. Change*, *29*(3), 293–309.
Hinkel, K. M., R. C. Frohn, F. E. Nelson, W. R. Eisner, and R. A. Beck (2005), Morphometric and spatial analysis of thaw lakes and drained thaw lake basins in the western Arctic Coastal Plain, Alaska, *Permafrost Periglac.*, *16*, 327–341.
Hinzman, L. D., et al. (2005), Evidence and implications of recent climate change in northern Alaska and other Arctic regions, *Clim. Change*, *72*, 251–298.
Hinzman, L. D., C. J. Deal, A. D. McGuire, S. H. Mernild, I. V. Polyakov, and J. E. Walsh (2013), Trajectory of the Arctic as an integrated system, *Ecol. Appl.*, *23*, 1837–1868.
Hishi, T., M. Hirobe, R. Tateno, and H. Takeda (2004), Spatial and temporal patterns of water-extractable organic carbon (WEOC) of surface mineral soil in a cool temperate forest ecosystem, *Soil Biol. Biochem.*, *36*(11), 1731–1737.
Hobara, S., K. Koba, N. Ae, A. E. Giblin, K. Kushida, and G. R. Shaver (2013), Geochemical Influences on Solubility of Soil Organic Carbon in Arctic Tundra Ecosystems, *Soil Sci. Soc. Am. J.*, *77*(2), 473–481.
Hodgkins, S. B., M. M. Tfaily, C. K. McCalley, T. A. Logan, P. M. Crill, S. R. Saleska, V. I. Rich, and J. P. Chanton (2014), Changes in peat chemistry associated with permafrost thaw increase greenhouse gas production, *Proc. Natl. Acad. Sci. U.S.A.*, *111*, 5819–5824.
Hubbard, S. S., et al. (2013), Quantifying and relating land-surface and subsurface variability in permafrost environments using LiDAR and surface geophysical datasets, *Hydrogeol. J.*, *21*, 149–169.
Huemmrich, K. F., G. Kinoshita, J. A. Gamon, S. Houston, H. Kwon, and W. C. Oechel (2010), Tundra carbon balance under varying temperature and moisture regimes, *J. Geophys. Res.*, *115*, G00I02, doi:10.1029/2009JG001237.
Intergovernmental Panel on Climate Change (2014), Climate Change 2013: The physical science basis: Working group I contribution to the fifth assessment report of the Intergovernmental Panel on Climate Change, Cambridge Univ. Press.
Jandl, R., and P. Sollins (1997), Water-extractable soil carbon in relation to the belowground carbon cycle, *Biol. Fertil. Soils*, *25*(2), 196–201.
Kotsyurbenko, O. R., K.-J. Chin, M. V. Glagolev, S. Stubner, M. V. Simankova, A. N. Nozhevnikova, and R. Conrad (2004), Acetoclastic and hydrogenotrophic methane production and methanogenic populations in an acidic West-Siberian peat bog, *Environ. Microbiol.*, *6*, 1159–1173.
Koven, C. D., B. Ringeval, P. Friedlingstein, P. Ciais, P. Cadule, and D. Khvorostyanov (2011), Permafrost carbon-climate feedbacks accelerate global warming, *Proc. Natl. Acad. Sci. U.S.A.*, *108*, 14,769–14,774.
Liljedahl, A. K., L. D. Hinzman, and J. Schulla (2012), Ice-wedge polygon type controls low-gradient watershed-scale hydrology, *Tenth International Conference on Permafrost*, *Salekhard*, *Russia*.
Lipson, D. A., M. Jha, T. K. Raab, and W. C. Oechel (2010), Reduction of iron (III) and humic substances plays a major role in anaerobic respiration in an Arctic peat soil, *J. Geophys. Res.*, *115*, G00I06, doi:10.1029/2009JG001147.
Lipson, D. A., D. Zona, T. K. Raab, F. Bozzolo, M. Mauritz, and W. C. Oechel (2012), Water-table height and microtopography control biogeochemical cycling in an Arctic coastal tundra ecosystem, *Biogeosciences*, *9*, 577–591.
Lipson, D. A., J. M. Haggerty, A. Srinivas, T. K. Raab, S. Sathe, and E. A. Dinsdale (2013a), Metagenomic insights into anaerobic metabolism along an Arctic peat soil profile, *PLoS One*, *8*, e64659.
Lipson, D. A., T. K. Raab, D. Goria, and J. Zlamal (2013b), The contribution of Fe(III) and humic acid reduction to ecosystem respiration in drained thaw lake basins of the Arctic Coastal Plain, *Global Biogeochem. Cycles*, *27*, 399–409, doi:10.1002/gbc.20038.
Lovley, D. R., and E. J. Phillips (1988), Novel mode of microbial energy metabolism: Organic carbon oxidation coupled to dissimilatory reduction of iron or manganese, *Appl. Environ. Microbiol.*, *54*(6), 1472–1480.
Mackelprang, R., M. P. Waldrop, K. M. DeAngelis, M. M. David, K. L. Chavarria, S. J. Blazewicz, E. M. Rubin, and J. K. Jansson (2011), Metagenomic analysis of a permafrost microbial community reveals a rapid response to thaw, *Nature*, *480*, 368–371.
McGuire, A. D., L. G. Anderson, T. R. Christensen, S. Dallimore, L. Guo, D. J. Hayes, M. Heimann, T. D. Lorenson, R. W. Macdonald, and N. Roulet (2009), Sensitivity of the carbon cycle in the Arctic to climate change of the carbon cycle in the Arctic to climate change sensitivity, *Ecol. Monogr.*, *79*, 523–555.
Metje, M., and P. Frenzel (2007), Methanogenesis and methanogenic pathways in a peat from subarctic permafrost, *Environ. Microbiol.*, *9*, 954–964.
Michaelson, G. J., and C. L. Ping (2003), Soil organic carbon and CO_2 respiration at subzero temperature in soils of Arctic Alaska, *J. Geophys. Res.*, *108*(D12), 8164, doi:10.1029/2001JD000920.
Mikan, C. J., J. P. Schimel, and A. P. Doyle (2002), Temperature controls of microbial respiration in arctic tundra soils above and below freezing, *Soil Biol. Biochem.*, *34*, 1785–1795.
Newman, B. D., et al. (2015), Microtopographic and depth controls on active layer chemistry in Arctic polygonal ground, *Geophys. Res. Lett.*, *42*, 1808–1817, doi:10.1002/2014GL062804.
Olefeldt, D., M. R. Turetsky, P. M. Crill, and A. D. McGuire (2013), Environmental and physical controls on northern terrestrial methane emissions across permafrost zones, *Global Change Biol.*, *19*, 589–603.
Riley, W. J., Z. M. Subin, D. M. Lawrence, S. C. Swenson, M. S. Torn, L. Meng, N. M. Mahowald, and P. Hess (2011), Barriers to predicting changes in global terrestrial methane fluxes: Analyses using CLM4Me, a methane biogeochemistry model integrated in CESM, *Biogeosciences*, *8*, 1733–1807.
Roden, E. E., and R. G. Wetzel (1996), Organic carbon oxidation and suppression of methane production by microbial Fe (III) oxide reduction in vegetated and unvegetated freshwater wetland sediments, *Limnol. Oceanogr.*, *41*, 1733–1748.
Roy Chowdhury, T., E. M. Herndon, T. J. Phelps, T. J. Phelps, D. A. Elias, B. Gu, L. Liang, S. D. Wullschleger, and D. E. Graham (2015), Stoichiometry and temperature sensitivity of methanogenesis and CO_2 production from saturated polygonal tundra in Barrow, Alaska, *Global Change Biol.*, *21*(2), 722–737.
Schädel, C., E. A. G. Schuur, R. Bracho, B. Elberling, C. Knoblauch, H. Lee, Y. Luo, G. R. Shaver, and M. R. Turetsky (2014), Circumpolar assessment of permafrost C quality and its vulnerability over time using long-term incubation data, *Global Change Biol.*, *20*, 641–652.

Schimel, J. P., and C. Mikan (2005), Changing microbial substrate use in Arctic tundra soils through a freeze-thaw cycle, *Soil Biol. Biochem.*, *37*, 1411–1418.
Schulz, S., and R. Conrad (1996), Influence of temperature on pathways to methane production in the permanently cold profundal sediment of Lake Constance, *FEMS Microbiol. Ecol.*, *20*, 1–14.
Schuur, E. A. G., et al. (2008), Vulnerability of permafrost carbon to climate change: Implications for the global carbon cycle, *BioScience*, *58*, 701.
Schuur, E. A. G., J. G. Vogel, K. G. Crummer, H. Lee, J. O. Sickman, and T. E. Osterkamp (2009), The effect of permafrost thaw on old carbon release and net carbon exchange from tundra, *Nature*, *459*, 556–559.
Shannon, R. D., and J. R. White (1996), The effects of spatial and temporal variations in acetate and sulfate on methane cycling in two Michigan peatlands, *Limnol. Oceanogr.*, *41*, 435–443.
Shaver, G. R., A. E. Giblin, K. J. Nadelhoffer, K. K. Thieler, M. R. Downs, J. A. Laundre, and E. B. Rastetter (2006), Carbon turnover in Alaskan tundra soils: effects of organic matter quality, temperature, moisture and fertilizer, *J. Ecol.*, *94*, 740–753.
Shiklomanov, N. I., D. A. Streletskiy, F. E. Nelson, R. D. Hollister, V. E. Romanovsky, C. E. Tweedie, J. G. Bockheim, and J. Brown (2010), Decadal variations of active-layer thickness in moisture-controlled landscapes, Barrow, Alaska, *J. Geophys. Res.*, *115*, G00I04, doi:10.1111/gcb.12417
Siegert, M., D. Cichocka, S. Herrmann, F. Gründger, S. Feisthauer, H. H. Richnow, D. Springael, and M. Krüger (2011), Accelerated methanogenesis from aliphatic and aromatic hydrocarbons under iron- and sulfate-reducing conditions, *FEMS Microbiol. Lett.*, *315*, 6–16.
Smith, L. C., Y. Sheng, G. M. MacDonald, and L. D. Hinzman (2005), Disappearing Arctic lakes, *Science*, *308*, 1429.
Solomon, D., J. Lehmann, J. Kinyangi, B. Liang, and T. Schafer (2005), Carbon K-edge NEXAFS and FTIR-ATR spectroscopic investigation of organic carbon speciation in soils, *Soil Sci. Soc. Am. J.*, *69*, 107–119.
Stolpe, B., L. Guo, A. M. Shiller, and G. R. Aiken (2013), Abundance, size distributions and trace-element binding of organic and iron-rich nanocolloids in Alaskan rivers, as revealed by field-flow fractionation and ICP-MS, *Geochim. Cosmochim. Acta*, *105*, 221–239.
Sturtevant, C. S., and W. C. Oechel (2013), Spatial variation in landscape-level CO_2 and CH_4 fluxes from Arctic coastal tundra: Influence from vegetation, wetness, and the thaw lake cycle, *Global Change Biol.*, *19*, 2853–2866.
Swift, R. (1996), Organic matter characterization, in *Methods of Soil Analyses Part 3—Chemical Methods*, edited by D. L. Sparks et al., Soil Sci. Soc. Am., Madison, Wis.
Tarnocai, C., J. G. Canadell, E. A. G. Schuur, P. Kuhry, G. Mazhitova, and S. Zimov (2009), Soil organic carbon pools in the northern circumpolar permafrost region, *Global Biogeochem. Cycles*, *23*, GB2023, doi:10.1029/2008GB003327.
Throckmorton, H. M., et al. (2015), Pathways and transformations of dissolved methane and dissolved inorganic carbon in Arctic tundra watersheds: Evidence from analysis of stable isotopes, *Global Biogeochem. Cycles*, doi:10.1002/2014GB005044.
Treat, C. C., et al. (2015), A pan-Arctic synthesis of CH_4 and CO_2 production from anoxic soil incubations, *Global Change Biol.*, *21*(7), 2787–2803.
Turetsky, M. R., C. C. Treat, M. P. Waldrop, J. M. Waddington, J. W. Harden, and A. D. McGuire (2008), Short-term response of methane fluxes and methanogen activity to water table and soil warming manipulations in an Alaskan peatland, *J. Geophys. Res.*, *113*, G00A10, doi:10.1029/2007JG000496
Weintraub, M. N., and J. P. Schimel (2003), Interactions between carbon and nitrogen mineralization and soil organic matter chemistry in Arctic tundra soils, *Ecosystems*, *6*, 129–143.
Weishaar, J. L., G. R. Aiken, B. A. Bergamaschi, M. S. Fram, R. Fujii, and K. Mopper (2003), Evaluation of specific ultraviolet absorbance as an indicator of the chemical composition and reactivity of dissolved organic carbon, *Environ. Sci. Technol.*, *37*, 4702–4708.
Western Regional Climate Center (2015), Barrow WSO Airport, Alaska (500546). [Available at http://www.wrcc.dri.edu/, (accessed January 2014).]
Wullschleger, S. D., L. D. Hinzman, and C. J. Wilson (2011), Planning the next generation of Arctic ecosystem experiments, *Eos AGU*, *92*, 145.
Zona, D., W. C. Oechel, J. Kochendorfer, K. T. Paw U, A. N. Salyuk, P. C. Olivas, S. F. Oberbauer, and D. A. Lipson (2009), Methane fluxes during the initiation of a large-scale water table manipulation experiment in the Alaskan Arctic tundra, *Global Biogeochem. Cycles*, *23*, GB2013, doi:10.1029/2009GB003487.
Zona, D., D. A. Lipson, R. C. Zulueta, S. F. Oberbauer, and W. C. Oechel (2011), Microtopographic controls on ecosystem functioning in the Arctic coastal plain, *J. Geophys. Res.*, *116*, G00I08, doi:10.1029/2009JG001241.